ACS Catalysis

pubs.acs.org/acscatalysis Research Article

Charge Transfer Drives Hydrogen Adsorption, Spillover, and Hydroxylation at the Pt/γ-Al_2O_3 Interface

George Yan,[§] Salman A. Khan,[§] and Dionisios G. Vlachos*

Cite This: *ACS Catal.* 2024, 14, 13579−13590 Read Online

ACCESS | Metrics & More | Article Recommendations | Supporting Information

ABSTRACT: Metal−support interactions have garnered much attention due to their impact on the structure and reactivity of supported metal catalysts. Despite the widespread recognition of multifunctional mechanisms in metal/metal oxide systems, much less attention has been paid to how the metal influences its support. Here, we explore metal−support interactions using hydrogen adsorption on a dehydroxylated γ-Al_2O_3(110) supported Pt_{10} cluster as a prototype. Through molecular dynamics simulations performed using an actively trained machine-learned force field, we observed reversible hydrogen spillover between the support and the metal. Analysis of the electronic structure and chemical nature of the interface reveals that charge transfer from H to the Pt_{10} cluster drives the spillover by stabilizing H adsorbed on the support. The same charge transfer concept also explains the stabilization of OH fragments at the Pt_{10}/γ-Al_2O_3(110) interface despite the scarcely impacted or even reduced acidity of interfacial Al sites. These findings demonstrate the rich chemistry of metal−support interfaces and the importance of "inverse" effects in the fundamental understanding of supported catalysts.

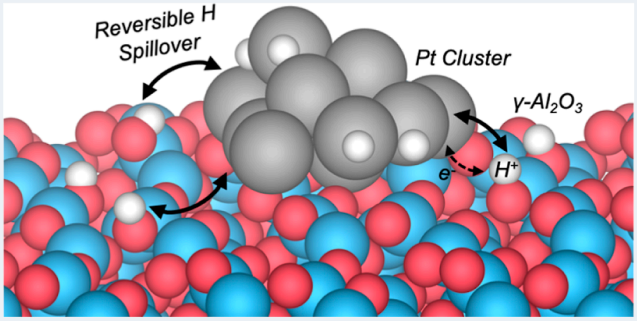

KEYWORDS: *metal−support interactions, surface hydroxylation, surface acidity, machine-learned force fields, active learning, molecular dynamics, density functional theory*

1. INTRODUCTION

Dispersed supported metal catalysts ranging from single atoms up to nanoparticles make up a large class of heterogeneous catalysts.[1] Fundamental investigations of supported metal catalysts have mainly focused on the chemistry over the active metal species. Modeling has employed contiguous metal surfaces for nanoparticle facets and homogeneous catalysis concepts for single atoms.[2,3] The importance of metal−support interactions has recently garnered much attention.[4−7] From interfacial charge transfer to encapsulation, an active support, such as CeO_2 or TiO_2, can alter the electronic and structural properties of a supported metal nanoparticle, modifying its catalytic properties.[8−12] Reactive metal/support interfacial sites had been demonstrated for various reactions, e.g., CO oxidation and water−gas shift.[13−18]

Metal atoms, clusters, and nanoparticles have also been reported to influence the structural and electronic properties of their support. On nonreducible supports, metals impact the nature, strength, and abundance of acidic sites, for instance, by binding to Lewis-acidic sites on γ-Al_2O_3 or by inducing reverse hydrogen spillover from hydroxyls on γ-Al_2O_3 and zeolites.[19−24] On reducible supports, metal-support interactions could influence the reducibility of the support, and induce phenomena such as the reverse spillover of oxygen.[4,25] These interactions are important for bifunctional catalysts, used for example in hydrocracking of hydrocarbons and plastics and hydrodeoxygenation of biomass, as some of the chemistry takes place on the support.[26−28] In light of the rich chemistry of metal/support interfaces, developing a wholistic picture of a working catalyst requires the consideration of these "inverse" effects of the dispersed metal species on its support.

Hydrogen is one of the most important industrial gases, and its activation permeates heterogeneous catalysis.[29,30] Several supported metal clusters are catalytically active for H_2 dissociation.[30−32] In some instances, dissociated H atoms can spillover onto the support initiating new catalytic mechanisms and consequently affecting activity and selectivity of the catalyst.[31,33] H spillover has been experimentally observed with spectroscopic methods, including IR,[34] NMR,[35] Raman,[36] etc. However, space- and time-averaged spectroscopic measurements cannot resolve adsorbate spillover dynamics and the spatial distribution of adsorbates on and around supported clusters.[37] Computational modeling can provide insight into

Received: June 13, 2024
Revised: August 21, 2024
Accepted: August 23, 2024

https://doi.org/10.1021/acscatal.4c03485
ACS Catal. 2024, 14, 13579−13590

the dynamics and distribution of dissociated H atoms and help interpret spectroscopic data.

In this work, we explore interfacial phenomena on a supported metal catalyst by examining the adsorption and spillover of hydrogen at the Pt/γ-Al_2O_3 interface through machine-learning-based molecular dynamics (MD) simulations and density functional theory (DFT) calculations. MD simulations demonstrate that H spillover at different coverages is dynamic, suggesting the possibility of reversible spillover and multiple catalytic pathways for reactions involving chemisorbed H. H spillover is accompanied by restructuring of the cluster and support, suggesting that catalyst sites are also dynamic under working conditions. DFT calculations confirmed the energetics of H adsorption and spillover at the Pt-alumina interface. Analysis of the adsorption and electronic structure of the interface reveals that charge transfer from H to low-lying unoccupied states of the Pt_{10} cluster in the alumina band gap enables spillover. By charge transfer from occupied states above the alumina valence band, a Pt_{10} cluster can also stabilize an OH fragment adsorbed near the Pt/γ-Al_2O_3 interface. The influence of support acidity was ruled out by comparing the adsorption energy of pyridine adsorbed on the Al sites near Pt.

Our paper is structured in the following way: we first examined the feasibility of hydrogen spillover by MD simulations and DFT calculations, followed by an analysis of the DFT calculations to elucidate the physical origin of the H spillover phenomenon. Finally, we demonstrate the generality of charge transfer-based stabilization of adsorbates by comparing H spillover to OH adsorption on the same surface and to similar phenomena in numerous systems.

2. METHODS

2.1. DFT Calculations and Structural Models. DFT calculations were performed using the Vienna Ab-initio Simulation Package, version 5.4.1.[38−40] The exchange−correlation (XC) energy was calculated using the Perdew−Burke−Ernzerhof (PBE) functional.[41] The DFT-D3 method with the Becke-Johnson damping function was used to calculate the van der Waals dispersion energy.[42,43] One electron wave functions were expanded using a basis set of plane waves with kinetic energy up to 400 eV. The core electrons were described using the projector-augmented wave method.[44] The electronic structure of the surface model in each self-consistent field (SCF) cycle was considered converged when the difference in total energy between consecutive SCF steps fell below 10^{-6} eV. The atomic positions were considered converged when the Hellmann−Feynman forces on unconstrained atoms fell below 0.02 eV/Å. The vibrational frequency calculations were performed using the finite difference method with a step size of 0.01 Å.

Two γ-Al_2O_3(110) slab models of different thickness were used in this work. Following our group's previous investigations, hydroxylation was not considered as the chemical potential of water is expected to be extremely low under a nonoxidative propane dehydrogenation reaction environment.[45] A 4-layer-thick γ-Al_2O_3(110) surface model was used to train the machine-learned force field, where the bottom layer of the model was fixed to bulk atomic positions. Spin polarization was not used in the 4-layer model calculations. All training calculations were performed in a (2 × 2) supercell of γ-Al_2O_3(110), where the dimensions of the simulation cell measure 16.7 Å × 16.0 Å × 20.0 Å. The Brillouin zone was sampled using a (2 × 2 × 1) Monkhorst−Pack mesh.[46] On the other hand, an 8-layer-thick γ-Al_2O_3(110) surface model was used to compute adsorption energies of radical fragments and probe molecules, for adsorption energy decomposition analyses, and for electronic structure analyses.[47−52] Spin polarization was used in the 8-layer model calculations. More details of the 8-layer model and comparisons between the two models are provided in the Supporting Information (see discussion in Section S1, Figures S1 and S2, Table S1). Finally, as a reference, the adsorption energies of hydrogen and OH on a (3 × 3) cell of Pt(111) were also computed. In these calculations, the Brillouin zone was sampled using a (9 × 9 × 1) Monkhorst−Pack mesh.

2.2. Moment Tensor-Based Machine Learning Potentials (MLPs). DFT calculations are prohibitively expensive, making it infeasible to simulate long-time scales for complex systems. Several advances in the past decade have enabled the development of readily parametrized accurate MLPs.[53] MLPs can model bond-breaking and -formation events and can be trained to a higher degree of accuracy compared to traditional force-fields.[54] Here we use moment tensor potentials (MTPs)[55] to perform MD simulations of H spillover in Pt/Al_2O_3. MTPs represent energies and forces in a basis of atom centered Chebyshev polynomials and moment tensor functions. MTPs are parametrized by fitting them to DFT calculated energies and forces on a set of representative atomistic configurations. MTPs can be trained to a high degree of accuracy with fewer configurations compared to other MLPs.[56] See ref 55 for details on the basis functions and the fitting procedure and Section S2 of the Supporting Information for details on MTP hyperparameters used for training.

2.3. Active Learning Procedure to Train MLPs and Molecular Dynamics (MD) Simulations. MTPs were trained with the active learning algorithm developed by Shapeev.[57] First, a preliminary MTP is trained on an initial set of randomly generated configurations. Active learning requires setting an extrapolation grade, γ, to actively choose configurations for retraining the MTP. γ measures the degree of extrapolation of an atomistic configuration from the training set. For details on defining γ see ref 57. Two thresholds of γ are required to be set for active learning, γ_{select} and γ_{break}. An MD simulation is performed with the preliminary MTP, and all configurations with $\gamma_{min} < \gamma < \gamma_{max}$ sampled during the MD run are stored for further retraining. The MD simulation is terminated if a configuration with $\gamma > \gamma_{max}$ is encountered and single-point DFT calculations are performed on the configurations stored in the database ($\gamma_{min} < \gamma < \gamma_{max}$). These configurations are added to the training set and the MTP is retrained. The MD simulation is restarted with the retrained MTP. Active learning stops once the MD simulation completes without encountering a configuration with $\gamma > \gamma_{min}$.

MTPs were trained for $H_{10}Pt_{10}$/γ-Al_2O_3. MD simulations were performed with the Large-scale Atomic/Molecular Massively Parallel Simulator code.[58] The equations of motion were integrated with the Velocity Verlet algorithm with a time step of 0.25 fs.[59] Simulations were performed in the *NVT* ensemble, and the temperature was controlled with a Langevin thermostat with a time constant of 0.1 ps.[60] γ_{set} and γ_{select} were set equal to 2.1 and 10.0, respectively. Active learning was terminated when no configurations with $\gamma > 2.1$ were encountered during a 10^6 step MD trajectory.

https://doi.org/10.1021/acscatal.4c03485
ACS Catal. 2024, 14, 13579−13590

3. RESULTS

3.1. Molecular Dynamics Simulations of a Hydrogen-Precovered Pt_{10} Cluster on γ-Al_2O_3(110). γ-Al_2O_3-supported Pt clusters are catalytically active for H_2 dissociation,[32] spilling over the dissociated H atoms onto the γ-Al_2O_3 support.[61] We investigated H spillover in Pt/γ-Al_2O_3 with 10 ns MD simulations at five different coverages with H/Pt ratios of 1, 0.8, 0.6, 0.4, and 0.2. MTP extrapolation errors for each coverage are reported in Table S2. The calculations were initialized with a stable Pt_{10}/γ-Al_2O_3(110) cluster obtained with basin-hopping.[62] We selected the Pt_{10} cluster as it has not been intensively studied on this surface and because the structural and combinatorial complexity of $Pt_{10}H_x$ makes it a good prototype for subnanometer clusters. H atoms were randomly dispersed on the Pt cluster, and the structure was locally optimized. We initialized simulations with different initial H atom configurations. In all cases, H atoms equilibrated over the Pt cluster within 2.5 ps, indicating that the initial H atom configuration does not influence the long-time dynamics of H spillover. All simulations were performed at 700 K to reflect industrial reaction temperatures involving Pt/γ-Al_2O_3 catalysts.[63]

Figure 1 shows the evolution of the average H−Pt, H−O, and H−Al coordination numbers, $\overline{CN}_{H-Pt}$, $\overline{CN}_{H-O}$, and

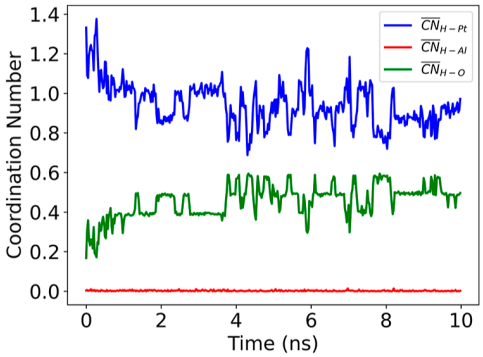

Figure 1. Average H−Pt, H−O, and H−Al coordination numbers as a function of time for a H/Pt coverage of 1:1. MD simulations were performed with a time step of 0.25 fs and configurations were dumped every 2000 steps. The plotted data was smoothed by averaging in blocks of 50 timesteps.

$\overline{CN}_{H-Al}$, respectively, for a H/Pt ratio of 1:1. Coordination numbers are averaged over all H atoms in a configuration. Cutoffs of 2.0, 1.2, and 1.9 Å were used for calculating H−Pt, H−O, and H−Al coordination numbers, respectively. Figure 2a shows the starting configuration of $H_{10}Pt_{10}$/γ-Al_2O_3(110), with all H atoms on the Pt_{10} cluster. Initially (t = 0), $\overline{CN}_{H-Pt}$ was approximately 1.4, because some H atoms were simultaneously coordinated with multiple Pt atoms. $\overline{CN}_{H-O}$ was approximately 0.2, despite no H atoms being coordinated to surface O atoms due to smoothing of the data. H atoms began to spillover from the Pt_{10} cluster onto γ-Al_2O_3 within 3 ps and contribute to the averaged point at t = 0. No H atoms were coordinated to Al atoms.

After the initial spillover at 3 ps, H atoms dynamically shuttled between the Pt cluster and surface O atoms near the cluster periphery, reflected in $\overline{CN}_{H-O}$ fluctuations between 0.2 and 0.4 within the first 1.5 ns. Following this, some H atoms diffused away from the cluster, and beyond 1.5 ns, $\overline{CN}_{H-O}$ fluctuated between 0.3 and 0.6. All spilled over H atoms

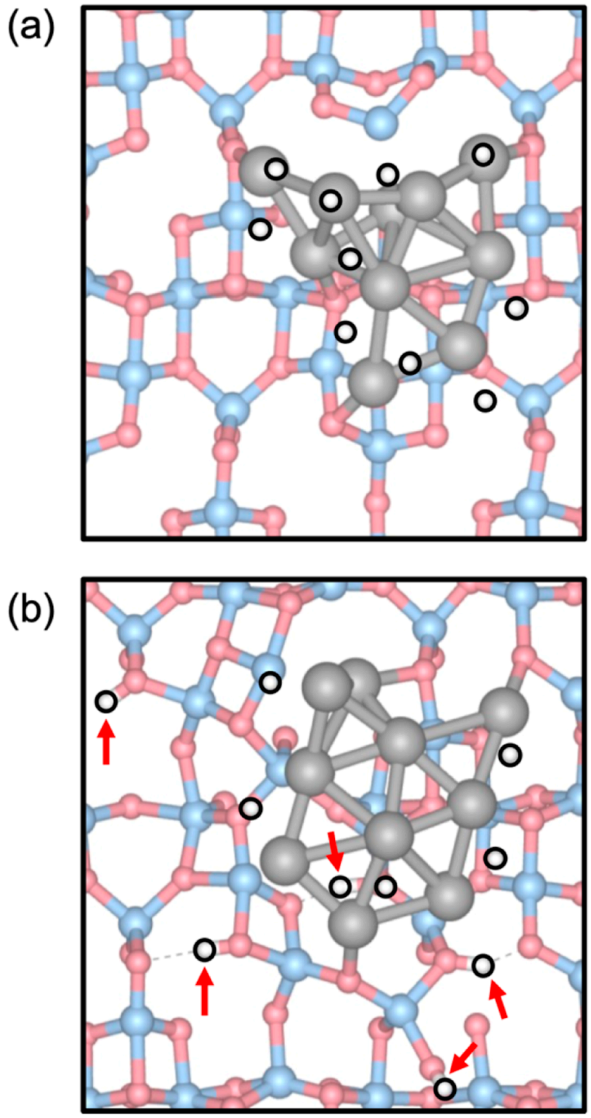

Figure 2. Configurations at the beginning and end of the 10 ns MD trajectory. (a) The initial configuration of $H_{10}Pt_{10}$/γ-Al_2O_3(110), with all H atoms are on top of the Pt cluster, and (b) the final configuration, where 5 of the 10 H atoms have spilled onto the Al_2O_3 support. Color scheme: Pt (gray), O (red), and Al (blue), and H (white with a black outline). Red arrows show spilled over H atoms.

coordinated with surface O atoms and no H−Al bonds were formed. Spilled over H atoms also hopped between adjacent support O atoms suggesting that they can diffuse across the support. Figure 2b shows the configuration at the end of the 10 ns trajectory, where 5 H atoms (marked with red arrows) have spilled over from the cluster onto the support, with one of those embedded between the cluster and the support by breaking a subsurface Al−O bond. In addition to H spillover, the initial 3D cluster transitioned to a flat geometry by 5 ns. Prior computational studies have also reported structural changes of gas-phase and supported metal clusters with temperature, e.g., Au,[64] Ag,[65] Cu,[65] Co,[66] Pt/α-Al_2O_3,[67] Au/CeO_2[68] etc. The 3D to flat transition of the Pt cluster is also accompanied by γ-Al_2O_3 restructuring, shown in Figure 2b. We also performed a 10 ns MD simulation with an extended (4 × 4) γ-Al_2O_3(110) slab to investigate the migration of H atoms away from the Pt_{10} cluster. However, we did not observe

https://doi.org/10.1021/acscatal.4c03485
ACS Catal. 2024, 14, 13579−13590

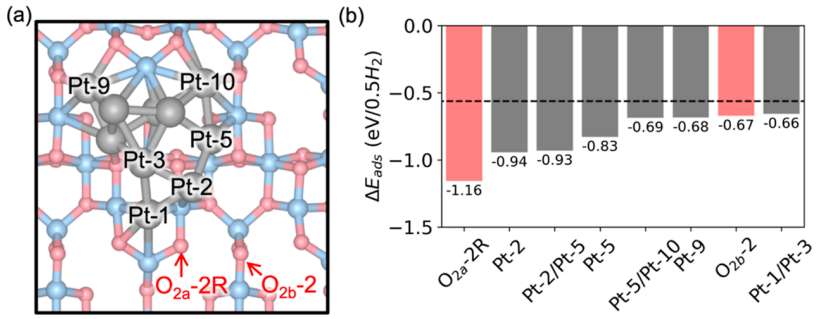

Figure 3. Adsorption energy (ΔE_{ads}) of hydrogen (H) on and surrounding the Pt_{10} cluster. (a) Geometry of the supported cluster and labeled Pt and O sites. (b) ΔE_{ads} of H (calculated with respect to H_2 gas) at the eight most stable sites. H prefers to adsorb on subcoordinated Pt sites (gray bars) and surface $O_{2a/b}$ sites surrounding the cluster (red bars). For reference, the ΔE_{ads} of H on Pt(111) is −0.56 eV at $\theta_H = 1/9$ and denoted with a horizontal dashed line in (b).

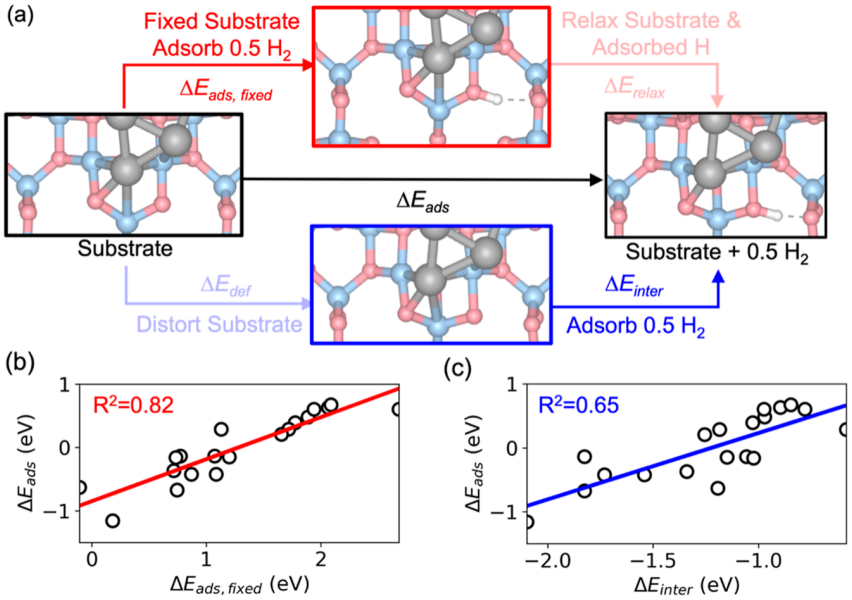

Figure 4. Adsorption energy decomposition analysis for the ΔE_{ads} of H on O sites surrounding the Pt_{10} cluster. (a) Energy decomposition schemes employed. (b) Correlation between the ΔE_{ads} of H on the Pt_{10}/γ-Al_2O_3 substrate, where the Pt_{10} cluster and the γ-Al_2O_3(110) surface were allowed to relax, and that where the cluster and surface were not allowed to relax ($\Delta E_{ads,fixed}$). (c) Correlation between ΔE_{ads} of H on the Pt_{10}/γ-Al_2O_3 substrate, where the Pt_{10} cluster and the γ-Al_2O_3(110) surface were allowed to relax, and that on the distorted Pt_{10}/γ-Al_2O_3 substrate (ΔE_{inter}). The Pt_{10} cluster enhances the intrinsic interaction strength between H and O sites near the Pt_{10}/γ-Al_2O_3(110) interface. H on O_{3a}-4R was omitted as an outlier due to subsurface Al reconstruction.

significant H migration far away from the Pt_{10} cluster, which indicates that spilled-over H atoms are more stable near the Pt/γ-Al_2O_3 interface and are unlikely to diffuse very far away after spillover. The evolution of coordination numbers at H/Pt coverages of 0.8:1, 0.6:1, 0.4:1, and 0.2:1 is shown in Figure S3. Similar to the 1:1 coverage, H atoms dynamically hop between the Pt cluster and the γ-Al_2O_3 support for all coverages.

3.2. Adsorption Energy of Hydrogen on Pt_{10}/γ-Al_2O_3(110). Motivated by the H spillover, we explored the adsorption energy of H on the O and Pt sites of Pt_{10}/γ-Al_2O_3(110) (Figure 3), calculated using an 8-layer model (see Methods and Section S1). Ordering the sites in ascending H adsorption energy (ΔE_{ads}, calculated with respect to H_2 gas), we found that H prefers to bind on the Pt-Top and Pt-Bri (bridge) sites of the cluster and the $O_{2a/b}$ sites surrounding it. Comparing all available Pt and O sites in the cell, we found that multiple O sites can bind H as strongly as Pt sites, with O sites immediately surrounding the Pt cluster as the most stable adsorption sites, consistent with results obtained from MD simulations (Figures S4−S6). H adsorbs most strongly on O_{2a}-2R, followed by atop Pt-2 and between Pt-2 and Pt-5 (Pt-2/Pt-5). This preference supports the H spillover to the $O_{2a/b}$ sites, as seen in the final image of the MD trajectory in Figure 2b.

In general, H adsorbs stronger on Pt_{10}/γ-Al_2O_3(110) than either Pt(111) or the bare γ-Al_2O_3(110) surface. Compared to the close-packed Pt(111) surface, H binds stronger on the Pt-2/Pt-5 bridge site by 0.37 eV. On the other hand, H adsorption on O_{2a}-2R is far stronger than that on a bare alumina surface, where the ΔE_{ads} of H on O_{2a} is 0.20 eV (Table S1). Among all O sites, although H prefers to bind to $O_{2a/b}$ than $O_{3a/b}$; its adsorption on $O_{3a/b}$ is still strongly stabilized compared to bare alumina (Figures S4−S6). Notably, H adsorption at the O_{3a}-2R site in a cavity under the Pt_{10} cluster is stabilized by 2.01 eV compared to the bare γ-Al_2O_3(110) surface (Figure S6), making the adsorption energy at this site comparable to that on Pt sites. This stabilization also agrees with the coordination of H under the Pt_{10} cluster, at the same

https://doi.org/10.1021/acscatal.4c03485
ACS Catal. 2024, 14, 13579−13590

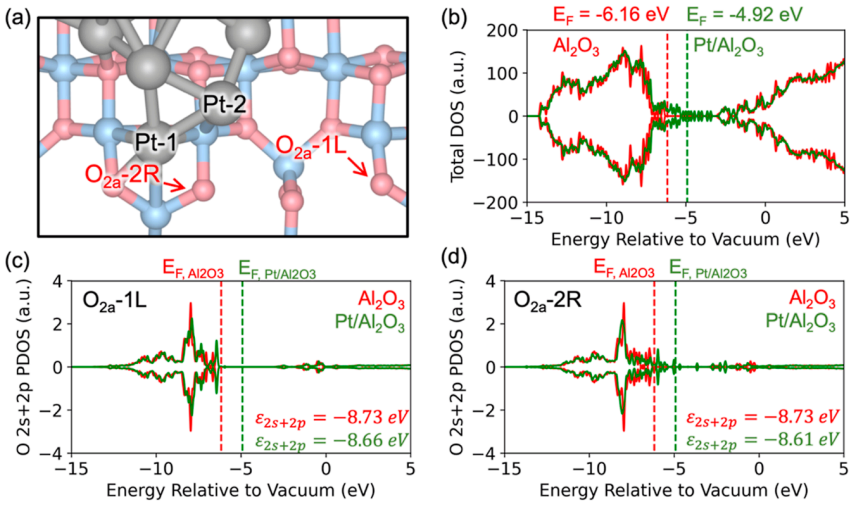

Figure 5. Electronic structure of the bare γ-$Al_2O_3(110)$ surface and Pt_{10}/γ-$Al_2O_3(110)$. (a) Geometry of the Pt_{10}/γ-$Al_2O_3(110)$ interface. (b) Electronic density of states (DOS) of bare γ-$Al_2O_3(110)$ and Pt_{10}/γ-$Al_2O_3(110)$. (c) O 2s + 2p PDOS of surface O_{2a}-1L on the bare γ-$Al_2O_3(110)$ surface (red) and on Pt_{10}/γ-$Al_2O_3(110)$ (green) and the first moment of their occupied O 2s+2p states (ε_{2s+2p}). (d) O 2s + 2p PDOS and ε_{2s+2p} of O_{2a}-2R on bare γ-$Al_2O_3(110)$ and Pt_{10}/γ-$Al_2O_3(110)$. The Pt_{10}/γ-$Al_2O_3(110)$ surface has a higher Fermi energy (E_F) than the bare γ-$Al_2O_3(110)$, where many states due to Pt are present in the alumina band gap. The interaction between O_{2a}-2R and Pt-1 pushes some O states above the E_F of the bare γ-$Al_2O_3(110)$, but the effect of Pt on unbound O (e.g., O_{2a}-1L) is limited.

site observed in the MD trajectories (Figure 2b). As both the flattening of the Pt_{10} cluster and additional γ-$Al_2O_3(110)$ surface reconstructions are observed in the MD trajectories, we also considered the adsorption of H on and near a flattened Pt_{10} cluster inserted between surface Al_{IVa} and O_{2a}. We found that neither the flattening nor the alternate surface reconstruction swayed the stabilization of H on these interfacial O sites (Figure S7). These deviations in the ΔE_{ads} of H relative to the reference surfaces suggest that H adsorption on Pt/Al_2O_3 intimately depends on the structure of the adsorption site.

In summary, H can adsorb strongly on the Pt_{10} cluster and the oxygens at its immediate support surroundings, making H spillover thermodynamically feasible. The ΔE_{ads} of H depends on the binding site, where $O_{2a/b}$ and Pt sites are largely preferred. Compared to the clean Pt(111) and γ-$Al_2O_3(110)$ surfaces, H adsorption on Pt_{10}/γ-$Al_2O_3(110)$ is much stronger.

3.3. Chemical Origin of the Strengthened Adsorption of Hydrogen. As atomic H binds weakly to O sites of nonreducible oxides, the strengthened ΔE_{ads} of H on O sites at and near the Pt_{10}/γ-$Al_2O_3(110)$ interface warrants a closer inspection. To uncover its chemical origin, we first studied the adsorbed state by energy decomposition analyses using two schemes (Figure 4). In both schemes, we partition the adsorption energy into two components, one which mainly represents the intrinsic interaction between the H and the O binding site, and another the extent to which the binding site must distort to host the adsorbed H. In the first scheme, the ΔE_{ads} of H on O sites was partitioned into that on a fixed Pt_{10}/γ-$Al_2O_3(110)$ substrate ($\Delta E_{ads,fixed}$) and the energy change of the subsequent structural relaxation (ΔE_{relax}). ΔE_{ads} is strongly correlated with $\Delta E_{ads,fixed}$, with a coefficient of determination (R^2) of 0.82. On the other hand, ΔE_{ads} and ΔE_{relax} are essentially uncorrelated, with R^2 of 0.14 (Figure S8a). In the second scheme, ΔE_{ads} was partitioned into the energy cost to distort the atomic positions of the Pt_{10}/γ-$Al_2O_3(110)$ substrate to those in the final H-adsorbed state (ΔE_{def}) and the subsequent adsorption energy of H on the distorted substrate (ΔE_{inter}). Here, ΔE_{ads} better correlates with ΔE_{inter} than ΔE_{def}, with R^2 of 0.65 and 0.40, respectively (Figures 4 and S8b). Both energy decomposition schemes suggest the intrinsic interaction strength between the H and the O sites near the Pt_{10} cluster, rather than creating more geometrically favorable H binding sites near the cluster, is responsible for enhancing ΔE_{ads}.

Since the intrinsic interaction between H and O sites best correlates with the ΔE_{ads} of H, we turn to investigate the chemical properties of the O sites on the Pt_{10}/γ-$Al_2O_3(110)$ surface and how they are influenced by Pt_{10}. By comparing the DOS of the bare γ-$Al_2O_3(110)$ and Pt_{10}/γ-$Al_2O_3(110)$, we found that Pt shifts the surface's Fermi energy (E_F) from −6.16 to −4.92 eV (Figure 5). The upshifted E_F is accompanied by the appearance of states in the γ-$Al_2O_3(110)$ surface band gap, which can mainly be assigned to Pt states with minor contributions from O and Al (see also the local DOS of relevant bands in Figure S9). An interfacial Pt−O bond can be characterized as a four-electron interaction between occupied states, which pushes some O 2s+2p states above the E_F of the bare γ-$Al_2O_3(110)$ due to Pauli repulsion and shifts the first moment of the occupied O 2s+2p states (ε_{2s+2p}) (Figures S10−S12).[69] Some upshifted O 2s+2p states (e.g., in O_{2a}-2R, Figure 5d) here may stabilize H on O bound to the Pt_{10} cluster. Although the Pt_{10} cluster has a pronounced effect on the electronic structure of O bound to it, its effect on surface O not bound to Pt_{10} is limited. The O 2s+2p PDOS of remote surface O resembles that on bare γ-$Al_2O_3(110)$, with few to no states above the E_F of the bare γ-$Al_2O_3(110)$ (e.g., in O_{2a}-1L, Figure 5c). The lack of upshifted 2s+2p states in the remote O sites cannot explain the strengthened ΔE_{ads} on these sites. Similarly, we found that the E_F of the flattened Pt_{10} cluster to be upshifted to −5.01 eV, demonstrating the generality of the phenomenon despite minor changes to the electronic structure due to the dynamical restructuring of the cluster and the support surface. Overall, although the Pt_{10} cluster directly affects the electronic structure of O sites to which it is bound, it has little impact on those not bound to the cluster.

https://doi.org/10.1021/acscatal.4c03485
ACS Catal. 2024, 14, 13579−13590

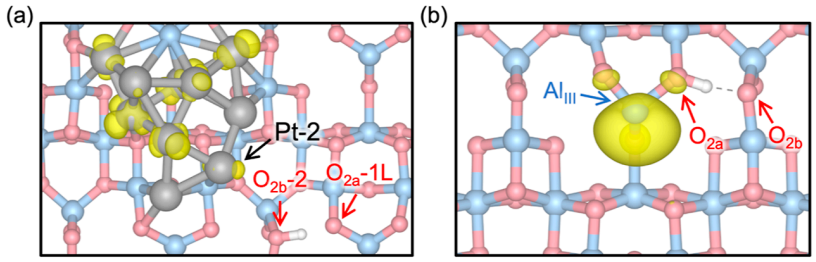

Figure 6. Charge transfer upon H adsorption on O. Spin density difference analysis for (a) H adsorption on the O_{2b}-2 site not bound to Pt_{10} and (b) on bare γ-Al_2O_3(110) (isosurface level of 0.003 a.u.; positive spin density is shown in yellow and negative in blue). H adsorption on O_{2b}-2 transfers charge to the Pt_{10} cluster, while charge is transferred to Al_{III} on the bare alumina. Unoccupied Pt states in the γ-Al_2O_3(110) band gap stabilizes H−O interactions by accepting charge from the adsorbed H.

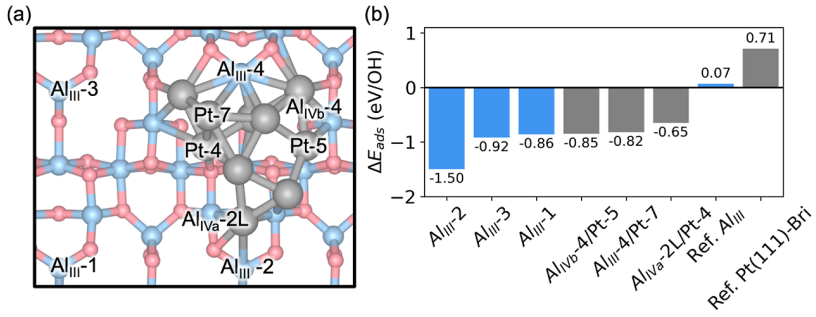

Figure 7. Charge transfer-stabilized adsorption of OH on surface Al sites surrounding the Pt_{10} cluster. (a) Geometry of the supported cluster and labeled Al sites. (b) Adsorption energy of an OH fragment on Al sites surrounding the Pt_{10} cluster and on a reference bare γ-Al_2O_3(110) and Pt(111) surface and (calculated with respect to H_2O and H_2 gas). Blue and gray bars denote adsorption on Al and Pt sites, respectively. Analogous to H on O, high-lying occupied Pt states enable the adsorption of OH on surface Al sites by donating charge to the adsorbed OH.

The spatially immediate effect of Pt−O bonding on the electronic structure of O sites cannot explain the stabilization of the ΔE_{ads} of H on O not bound to the cluster. To better understand the longer-ranged effects of the Pt_{10} cluster, we analyzed the spin density difference for H adsorption. Specifically, we compared H adsorbed on the O_{2b}-2 site of Pt_{10}/γ-Al_2O_3(110) (O_{2b}-2 is not bound to Pt) and O_{2a} site of the bare γ-Al_2O_3(110) surface (Figure 6). When H adsorbs on O_{2b}-2, charge is mainly transferred to the Pt_{10} cluster, which is expressed as diffuse lobes of positive spin density difference on the cluster. On the other hand, upon H adsorption on O_{2a} of the bare γ-Al_2O_3(110) surface, charge is transferred to the lowest unoccupied band of the adjacent Al_{III} (see also LDOS in Figure S9), resembling the adsorption of atomic H on coordinatively unsaturated sites of MgO.[70,71] The different charge transfer behaviors are due to the electronic structure of the surfaces. Pt_{10}/γ-Al_2O_3(110) has many low-lying unoccupied Pt states in the alumina surface band gap and readily accommodates the excess charge. In contrast, the conduction band of the bare γ-Al_2O_3(110) surface cannot as it is much higher in energy. A similar behavior is observed upon H adsorption on fixed Pt_{10}/γ-Al_2O_3(110) and γ-Al_2O_3(110) surfaces, which, in combination with the adsorption energy decomposition analysis presented above, suggest that charge transfer to Pt_{10} is the main mechanism behind the stabilization (Figures 4 and S13). This mechanism is consistent with the diminished stability of spilled-over H on O sites farther away from the Pt cluster due to charge separation (e.g., O_{3a}-1L/R vs O_{3a}-3L/R, Figure S6). Although H_2 can dissociate on the bare γ-Al_2O_3(110) surface to form an OH with lattice O, the reaction is heterolytic, and one H^- must form on Al to balance the charge.[72] Near the Pt/γ-Al_2O_3 interface, unoccupied states below the γ-Al_2O_3 conduction band belonging to the Pt cluster act as the countercharge for H^+ instead.

3.4. Charge Transfer-Based Stabilization of OH Near the Pt-Alumina Interface. As an immediate extension of the charge transfer-based H stabilization on surface O, one may hypothesize that the high-lying occupied Pt states above the γ-Al_2O_3 valence band may serve as the countercharge for an anionic fragment. As a proof-of-concept, we compared the ΔE_{ads} of an OH fragment on Pt and Al_{III} sites (with respect to H_2O and H_2 gas) against that on Pt(111) and on the Al_{III} site of γ-Al_2O_3(110) (Figures 7 and S14). Overall, OH is bound stronger at the interfacial Al_{III} sites than at Pt−Al bridge sites or the Pt cluster. The most stable adsorption sites were Al_{III}-2, followed by Al_{III}-3 and Al_{III}-1. Compared to the bare γ-Al_2O_3(110) surface, an OH adsorbed at Al_{III}-2 is stabilized by 1.57 eV. By visualizing the spin density difference, we found that charge is transferred from the Pt_{10} cluster to the OH fragment upon adsorption (Figure S15). On the other hand, upon OH adsorption on Al_{III} of the bare γ-Al_2O_3(110) surface, charge is transferred out of the low-coordinate $O_{2a/b}$ sites, whose occupied states lie lower in energy than the Pt states, rendering the adsorption much less favorable. These results demonstrate that the Pt cluster can also act as the countercharge to stabilize an anionic fragment near the Pt-alumina interface.

Analogous to H adsorption on O, it is also possible that the strengthened OH adsorption near the Pt_{10} cluster is due to the inherent differences in the Lewis acidity of Al sites in the presence of the cluster. To probe the intrinsic Lewis acidity of surface Al sites, we compared the energy position of the unoccupied Al 3s + 3p states. Like surface O, bonding between surface Al and the Pt_{10} cluster affects the Al site's electronic

https://doi.org/10.1021/acscatal.4c03485
ACS Catal. 2024, 14, 13579−13590

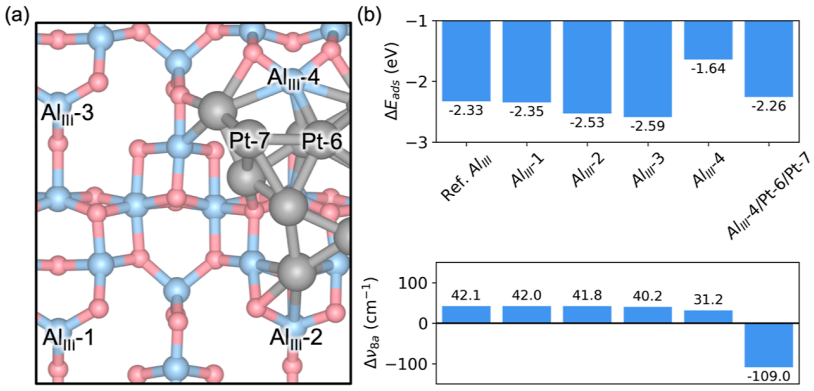

Figure 8. Pyridine adsorption on Al_{III} sites in the presence of Pt. (a) Cluster geometry and labels of Al sites. (b) Adsorption energy of pyridine on sites shown in (a) and shifts in the "8a" vibrational mode of adsorbed pyridine compared to reference structures. The Lewis acidity of Al_{III}-4 is reduced, but those not bound to Pt are scarcely affected. Pyridine could also adopt a flat, multidentate configuration on Al_{III}-4 and the surrounding Pt.

structure, forming new unoccupied states below the conduction band. In contrast, the electronic structure of remote Al sites resembles the bare γ-Al_2O_3(110) and should not stabilize OH (Figure S16). The Al−Pt interaction can be characterized as a two-electron one with primarily bonding character (Figure S17).

As a second comparison, we calculated the ΔE_{ads} of pyridine and shifts in the "8a" vibrational mode of adsorbed pyridine on the available Al sites of Pt_{10}/γ-Al_2O_3(110) (Figures 8 and S18, and Table S3), as an extrinsic measure of Lewis acidity. Here, we target monodentate adsorption modes that only involve Al−N interactions as a metric for acidity. The ΔE_{ads} of pyridine at the Al_{III}-4, Al_{IV_a}-2L, Al_{IV_b}-3, and Al_{IV_b}-4 sites weakens by 0.1 eV or more, while the ΔE_{ads} of pyridine at the Al_{III}-2, Al_{III}-3, Al_{IV_a}-1R, Al_{IV_a}-3L, and Al_{IV_b}-2 sites strengthens by 0.1 eV or more. The shifts in the ΔE_{ads} of pyridine are accompanied by marginal differences in the blueshift of the pyridine "8a" vibrational mode. Overall, these relatively minor differences in the extrinsic acidity of Al sites in the presence of Pt are incommensurate with the much larger stabilization of OH observed above, leaving charge transfer as the primary mechanism.

A loss of acidity, though, does not necessarily mean a loss in reactivity. When adsorbed on Al sites sufficiently close to Pt_{10}, pyridine can be further stabilized by adopting a multidentate configuration, with the aromatic ring partially adsorbed on Pt sites (Figure S19). For instance, although the ΔE_{ads} of pyridine at the Al_{III}-4 site in an upright configuration is much weaker than on an ordinary Al_{III} site (−1.64 vs −2.33 eV), bonding between the aromatic ring and the adjacent Pt-6 and Pt-7 can stabilize this multifunctional adsorbate. Here, the 8a vibrational mode is severely red-shifted due to bonding between the π system of the aromatic ring and the Pt cluster. These configurations are reminiscent of the flatter pyridine adsorption geometries on Pt(111) at low temperatures and coverage.[73,74]

4. DISCUSSION

4.1. Dynamics of Hydrogen Spillover on Pt/γ-Al_2O_3. Space- and time-averaged spectroscopic methods cannot directly probe the spillover dynamics and distribution of H on supported metal clusters. MD can simulate H spillover dynamics and spatial distribution and help interpret spectroscopic measurements. However, most computational studies of H spillover have used expensive ab initio MD simulations limited to a few picoseconds.[75−77] Recent advances in MLPs enable longer time scale MD simulations at ab initio accuracy to provide critical insight into slower processes associated with hydrogen spillover.

Our computations suggest that H spillover can occur across a range of H coverages, notably even at low coverages of H/Pt = 0.2. Spilled-over H atoms can embed themselves between the Pt cluster and Al_2O_3 support, creating potentially new hydrogen storage and catalysis mechanisms. Furthermore, H spillover between the metal and the support is dynamic and reversible, suggesting reverse spillover and additional catalytic pathways for hydrogen-involving reactions.

Simulations also show Pt cluster and Al_2O_3 support restructuring at longer time scales, which could affect reaction kinetics and thermodynamics. The Pt cluster flattens as it restructures, leading to increased Pt dispersion. The restructuring also alters the local coordination environment of Al and O sites bonded to Pt. These changes can affect the acid/base properties of the interface and the kinetics of typical Lewis acid-catalyzed reactions, which will be the subject of future investigations.

Our work underscores the importance of exploring long-time scale processes associated with H spillover on Pt/Al_2O_3 catalysts inaccessible by expensive ab initio MD simulations.

4.2. Mechanism of H Spillover and Energetics of H_2 Chemisorption on Pt/γ-Al_2O_3. The spillover of hydrogen on supported metal catalysts has been studied for decades. Although generally considered much less favorable on nonreducible oxides than reducible ones, H spillover from Pt nanoparticles to nonreducible oxides has been demonstrated in model systems with well-defined structures.[78−81] The difficulty stems from the weak adsorption of atomic H on nonreducible oxides, whereas on reducible oxides, H could be stabilized by donating its electron to the support.[78] H spillover on nonreducible oxides is believed to be assisted by defects on the support, Brønsted acid sites, or H^+ diffusion coupled with that of an anionic fragment, such as H^-.[33,78,79] The charge transfer-based mechanism in our work shares a similarity with the proposed mechanisms, in that spilled-over H prefers binds to undercoordinated O sites present on the dehydroxylated γ-Al_2O_3(110) support. Such surface Al and O sites (termed "defect sites") have been reported to activate H_2 and alkanes through a Lewis acid−base mechanism.[45,72] H spillover was

https://doi.org/10.1021/acscatal.4c03485
ACS Catal. 2024, 14, 13579−13590

not observed on Pt clusters supported on other dehydroxylated alumina facets and hydroxylated γ-Al_2O_3(110); though, reverse H spillover from hydroxylated γ-Al_2O_3(110) to Pt clusters has been reported at low H coverages.[67,82−84] Importantly, our mechanism differs from the proposed mechanisms as it accounts for the electronic influence of the supported metal species. The presence of the Pt_{10} cluster is vital as it avoids the unfavorable charge transfer to Al sites on the alumina support (Figure 6). This distinction demonstrates the importance of the supported metal species on its support. Overall, we expect the charge-transfer-driven mechanism to be responsible for H spillover near the Pt/γ-Al_2O_3 interface, as charge separation will diminish the stability of spilled-over H farther away. We recognize that the presence of undercoordinated O sites on the support and low-lying unoccupied electronic states on the cluster are conducive for spillover at the Pt/γ-Al_2O_3 interface.

Beyond the spillover of H, the chemisorption of hydrogen on Pt/γ-Al_2O_3 has also been studied for decades, and several assignments have been proposed for the various adsorption sites. Based on reported temperature-programmed desorption spectra of H_2-treated Pt/γ-Al_2O_3, H_2 desorption peaks beyond the reversibly bound H_2 desorption peak in the range of 100−200 °C have been assigned to H adsorbed at the Pt-alumina interface, H spilled over to alumina, H adsorbed at subcoordinated Pt sites, or Pt-catalyzed decomposition of OH groups or surface impurities.[61,82,83,85] The calculated energetics of H spillover in this work support that both H adsorbed on subcoordinated Pt sites and O at the Pt/γ-Al_2O_3(110) interface (Figure 3) could contribute to high-temperature H_2 desorption peaks. Our results also have ramifications regarding the interpretation of calorimetric and surface site titration studies.

4.3. Electronic Structure of Pt/γ-Al_2O_3 and Charge Transfer Near Metal−Support Interfaces. By analyzing the influence of Pt on the adsorption of H, OH, and pyridine, we found that charge transfer involving Pt states in the γ-Al_2O_3(110) surface band gap stabilizes adsorbates on O and Al sites not bound to Pt. The presence of these states is directly related to the heightened E_F of Pt_{10}/γ-Al_2O_3(110) compared to both contiguous Pt surfaces and γ-Al_2O_3(110). This difference is mainly due to the coordinatively unsaturated geometry of the Pt_{10} cluster; a similar rise in the E_F is also reported for γ-Al_2O_3-supported Pd_4 clusters.[19] More generally, the electronic structure of Pt/γ-Al_2O_3 can be compared to that of a metal−insulator heterojunction.[86,87] At the heterojunction interface, the Fermi energy could be raised due to electrostatic compression, charge transfer, and structural relaxation.[88] States in the insulator band gap can be formed due to the decay of the metal wave function into the insulator medium, chemical bonding, and charge transfer.[89] Here, aside from the presence of high-lying Pt states corresponding to coordinatively unsaturated Pt sites, states above the E_F of the bare γ-Al_2O_3(110) surface are also generated due to Pt−Al and Pt−O interactions (Figure 5). The formation of these additional states falls under gap states induced by chemical bonding, where the bonding picture is consistent with reported analyses of γ-Al_2O_3 supported Pd and Pt clusters.[19,23,67] Although the upshifted O 2p states could contribute to the strengthened adsorption of H at the Pt-γ-Al_2O_3 interface, they cannot explain the stabilization on the O sites farther away from the interface.

An important class of heterogeneous catalysts often likened to a heterojunction is the inverse catalyst, where the spatially immediate influence of the Pt cluster on the electronic structure of alumina resembles that observed on MgO(100) thin films.[89,90] Although 1 and 2 monolayer (ML) thick MgO(100) films deviate from thicker films due to the quantum size effect, the electronic properties of the both supported and unsupported MgO(100) film begin to resemble that of thick films from the third ML onward; the adsorption energy and structure of single Pd, Ag, and Au atoms on unsupported MgO(100) surfaces are already converged by the third ML.[89,91,92] In relation, the minorly impacted acid/base properties of Al and O sites away from the Pt-γ-Al_2O_3 interface (Figures 5, S10, and S16) are comparable to those of MgO, where the adsorption energy of a neutral Pd atom has been reported to be similar on both supported and unsupported thick MgO(100) films.[92]

Beyond the electronic structure and acid/base properties, the adsorbate charge transfer observed near the Pt/γ-Al_2O_3 interface is comparable to reported findings in conventional catalysts. The stabilization of H^+ on tetragonal ZrO_2(101) in the presence of a Ru_{10} cluster (although still less stable than H on Ru_{10} at low coverage) and of anionic fragments on MgO(100) in the presence of a metal rod have been reported.[17,93−95] Analyses of these systems paint a familiar physical picture, where charge transfer to/from the metal species is responsible for the stabilization.[94] In the desorbing direction, the formation of oxygen vacancies (V_O) on nonreducible oxides has also been reported to benefit from the presence of a metal species, such as that in the presence of a Ru_{10} cluster, which becomes more endothermic with distance from the cluster.[4] Besides charge transfer, the V_O could also be stabilized by bonding between the metal atom/cluster and the cations surrounding the V_O.[96−98] This bonding contribution is reminiscent of the H adsorption, as certain upshifted O 2p states of O bound to the Pt_{10} cluster may stabilize the adsorbed H (e.g., O_{2a}-2R).

Aside from conventional catalysts, adsorbate charge transfer has also been reported on inverse catalysts. When a metal−supported MgO(100) film is sufficiently thin (ca. 3 ML or less), electrons can tunnel through it to stabilize compatible adsorbates, including H^+.[99−101] Like the case of spilled-over H, these adsorbates become less stable with increasing MgO film thickness due to charge separation.[99] One difference between H adsorption near the Pt-alumina interface and charge transfer through MgO(100) thin films is the dependence on site structure. The adsorption of an Au adatom on MgO(100) thin films is facilitated by a strong inward relaxation of the Mg site.[99,102] Importantly, the charging of Au is diminished without surface relaxation, while charge transfer from H to the Pt_{10} cluster does not require relaxation (Figure S13). These differences suggest that adsorbate charge transfer is heavily dependent on the structure of the metal-oxide interface and the identity of the adsorbate.

4.4. Catalytic Reactions Over Supported Metal Catalysts. The chemical and electronic properties of the Pt-alumina interface, which stabilize radicals on the support, have several implications for reactions on supported metal catalysts. Bifunctional mechanisms have been recognized for reactions such as hydrocracking and hydrodeoxygenation.[26,27] Scaling relations-based kinetic analyses of bifunctional catalysts had been reported, which identified situations where the spillover of adsorbates could improve the catalyst's overall reactivity.[103,104] Importantly, the reported analyses show that rapid diffusion and spillover of intermediates is required for a

https://doi.org/10.1021/acscatal.4c03485
ACS Catal. 2024, 14, 13579−13590

multicomponent catalyst to outperform the sum of its parts. Here, rapid, reversible H spillover was realized due to charge transfer at the Pt/γ-Al_2O_3(110) interface and may be generalized to other nonreducible supports, as discussed above, provided that the electronic structure of the interface readily facilitates charge transfer and that reactive sites are present on the support near the metal cluster. Spilled-over H may influence the reactivity and selectivity of (de)-hydrogenation reactions over such catalysts, as they allow elementary (de)hydrogenation steps to occur at sites where H_2 activation may be difficult. For instance, aluminosilicate-encapsulated Pt catalysts have been reported to be active for cyclohexane/benzene (de)hydrogenation due to H spillover enabling reaction on support sites but less active for propane hydrogenolysis.[79] The thermodynamics of H adsorption may also influence the coverage of H on the cluster and the interface, as the coverage of H on Pd and Pt surfaces had been reported to influence the selectivity of furfural hydrogenation and propane dehydrogenation.[105,106]

Another possible consequence originates from the proximity of metal and acidic sites, where structure-sensitive reactions involving a multidentate species could benefit. As reported for CO oxidation over supported Au catalysts and dry reforming of methane over Ni/γ-Al_2O_3, important intermediates and transition states can be stabilized at the metal−support interface.[14,15,107−109] We observed a similar result here in the adsorption of pyridine; the lone pair on N and the conjugated C could simultaneously bind to Al and Pt, respectively (Figure 8). The adsorption energy of pyridine in this configuration is comparable to or greater than that on standalone Al_{III} and $Al_{IVa/b}$ sites. Another important consequence, as reported for MgO-supported metal rods, is that linear scaling relations at the metal-oxide boundary often differ from those on monometallic surfaces, which may also promote multistep reactions occurring through bifunctional mechanisms, as discussed above.[94,95]

5. CONCLUSIONS

In this work, we explored the adsorption and spillover of hydrogen on a Pt_{10} cluster supported on dehydroxylated γ-Al_2O_3(110) through MD simulations using a MLP and DFT-based electronic structure calculations. MD simulations show that H spillover is reversible and occurs at various coverages. H spillover is also accompanied by a restructuring of the Pt cluster and the γ-Al_2O_3(110) support at higher temperatures, indicating that the catalyst site structure dynamically evolves at higher temperatures. Through DFT-based H adsorption energy calculations, we found that aside from coordinatively unsaturated Pt sites on the Pt_{10} cluster, $O_{2a/b}$ sites at and near the Pt-γ-Al_2O_3 interface could also serve as potent binding sites for H, which enable the spillover of H from the Pt_{10} cluster to alumina at a modest H coverage. By adsorption energy decomposition and electronic structure analyses, we showed that reactive Pt states near the Fermi energy of Pt_{10}/γ-Al_2O_3(110) are primarily responsible for the stabilization of H near the Pt-alumina interface. We further demonstrated the charge transfer-driven stabilization of charged fragments by comparing the adsorption energy of OH near the Pt-alumina interface to that on a bare γ-Al_2O_3(110) surface. Finally, through pyridine adsorption calculations, we showed that surface Al sites not bound to the Pt_{10} cluster retain their Lewis acidity, and the proximity of Pt and Al sites stabilizes multidentate adsorbates. Our work demonstrates that the unique electronic structure of the metal−support interface enables redox reactions otherwise unachievable over a nonreducible but active support. These results also show that the metal affects the chemical properties of its support. Moreover, our framework, combining MLPs and electronic structure calculations, can be readily applied to investigate H spillover for other supported metal catalysts.

■ ASSOCIATED CONTENT

Supporting Information

The Supporting Information is available free of charge at https://pubs.acs.org/doi/10.1021/acscatal.4c03485.

Additional details of structural models, MLP parametrization, H, OH, and pyridine adsorption energetics, and electronic structure analyses (PDF)

Geometry, total energy, and vibrational frequencies of intermediates referenced in this work (ZIP)

Trained MTP and training data (ZIP)

■ AUTHOR INFORMATION

Corresponding Author

Dionisios G. Vlachos − *Delaware Energy Institute, University of Delaware, Newark, Delaware 19716, United States; Department of Chemical and Biomolecular Engineering, University of Delaware, Newark, Delaware 19716, United States;* orcid.org/0000-0002-6795-8403; Email: vlachos@udel.edu

Authors

George Yan − *Delaware Energy Institute, University of Delaware, Newark, Delaware 19716, United States;* orcid.org/0009-0002-3870-5447

Salman A. Khan − *Delaware Energy Institute, University of Delaware, Newark, Delaware 19716, United States*

Complete contact information is available at: https://pubs.acs.org/10.1021/acscatal.4c03485

Author Contributions

[§]G.Y. and S.A.K. equal contributions.

Notes

The authors declare no competing financial interest.

■ ACKNOWLEDGMENTS

This work was supported by the National Science Foundation's "Designing Materials to Revolutionize and Engineer our Future" (DMREF) program under Award number 2323700. This research was also partly supported by the high-performance computing resources of the Information Technologies (IT) at the University of Delaware. The authors thank Dr. Stavros Caratzoulas for helpful discussions and feedback on the manuscript.

■ REFERENCES

(1) Liu, L.; Corma, A. Metal catalysts for heterogeneous catalysis: from single atoms to nanoclusters and nanoparticles. *Chem. Rev.* **2018**, *118* (10), 4981−5079.

(2) Van Santen, R. A. Complementary structure sensitive and insensitive catalytic relationships. *Acc. Chem. Res.* **2009**, *42*, 57−66.

(3) Copéret, C.; Comas-Vives, A.; Conley, M. P.; Estes, D. P.; Fedorov, A.; Mougel, V.; Nagae, H.; Núñez-Zarur, F.; Zhizhko, P. A. Surface Organometallic and Coordination Chemistry toward Single-Site Heterogeneous Catalysts: Strategies, Methods, Structures, and Activities. *Chem. Rev.* **2016**, *116* (2), 323−421.

(4) Ruiz Puigdollers, A.; Schlexer, P.; Tosoni, S.; Pacchioni, G. Increasing Oxide Reducibility: The Role of Metal/Oxide Interfaces in the Formation of Oxygen Vacancies. *ACS Catal.* **2017**, *7* (10), 6493−6513.
(5) Ro, I.; Resasco, J.; Christopher, P. Approaches for Understanding and Controlling Interfacial Effects in Oxide-Supported Metal Catalysts. *ACS Catal.* **2018**, *8* (8), 7368−7387.
(6) van Deelen, T. W.; Hernández Mejía, C.; de Jong, K. P. Control of metal-support interactions in heterogeneous catalysts to enhance activity and selectivity. *Nat. Catal.* **2019**, *2* (11), 955−970.
(7) Xu, M.; Peng, M.; Tang, H.; Zhou, W.; Qiao, B.; Ma, D. Renaissance of Strong Metal−Support Interactions. *J. Am. Chem. Soc.* **2024**, *146* (4), 2290−2307.
(8) Tauster, S. J.; Fung, S. C. Strong metal-support interactions: occurrence among the binary oxides of groups IIA−VB. *J. Catal.* **1978**, *55* (1), 29−35.
(9) Valden, M.; Lai, X.; Goodman, D. W. Onset of Catalytic Activity of Gold Clusters on Titania with the Appearance of Nonmetallic Properties. *Science* **1998**, *281* (5383), 1647−1650.
(10) Bruix, A.; Rodriguez, J. A.; Ramírez, P. J.; Senanayake, S. D.; Evans, J.; Park, J. B.; Stacchiola, D.; Liu, P.; Hrbek, J.; Illas, F. A new type of strong metal−support interaction and the production of H2 through the transformation of water on Pt/CeO2(111) and Pt/CeOx/TiO2(110) catalysts. *J. Am. Chem. Soc.* **2012**, *134* (21), 8968−8974.
(11) Lykhach, Y.; Kozlov, S. M.; Skála, T.; Tovt, A.; Stetsovych, V.; Tsud, N.; Dvořák, F.; Johánek, V.; Neitzel, A.; Mysliveček, J. Counting electrons on supported nanoparticles. *Nat. Mater.* **2016**, *15* (3), 284−288.
(12) Frey, H.; Beck, A.; Huang, X.; van Bokhoven, J. A.; Willinger, M. G. Dynamic interplay between metal nanoparticles and oxide support under redox conditions. *Science* **2022**, *376* (6596), 982−987.
(13) Fu, Q.; Li, W.-X.; Yao, Y.; Liu, H.; Su, H.-Y.; Ma, D.; Gu, X.-K.; Chen, L.; Wang, Z.; Zhang, H.; Wang, B.; Bao, X. Interface-Confined Ferrous Centers for Catalytic Oxidation. *Science* **2010**, *328* (5982), 1141−1144.
(14) Green, I. X.; Tang, W.; Neurock, M.; Yates, J. T., Jr. Insights into Catalytic Oxidation at the Au/TiO2 Dual Perimeter Sites. *Acc. Chem. Res.* **2014**, *47* (3), 805−815.
(15) Saavedra, J.; Doan, H. A.; Pursell, C. J.; Grabow, L. C.; Chandler, B. D. The critical role of water at the gold-titania interface in catalytic CO oxidation. *Science* **2014**, *345* (6204), 1599−1602.
(16) Shekhar, M.; Wang, J.; Lee, W.-S.; Williams, W. D.; Kim, S. M.; Stach, E. A.; Miller, J. T.; Delgass, W. N.; Ribeiro, F. H. Size and Support Effects for the Water−Gas Shift Catalysis over Gold Nanoparticles Supported on Model Al2O3 and TiO2. *J. Am. Chem. Soc.* **2012**, *134* (10), 4700−4708.
(17) Zhao, Z.-J.; Li, Z.; Cui, Y.; Zhu, H.; Schneider, W. F.; Delgass, W. N.; Ribeiro, F.; Greeley, J. Importance of metal-oxide interfaces in heterogeneous catalysis: A combined DFT, microkinetic, and experimental study of water-gas shift on Au/MgO. *J. Catal.* **2017**, *345*, 157−169.
(18) Shekhar, M.; Lee, W.-S.; Akatay, M. C.; Maciel, L.; Tang, W.; Miller, J. T.; Stach, E. A.; Neurock, M.; Delgass, W. N.; Ribeiro, F. H. Water-gas shift reaction over supported Au nanoparticles. *J. Catal.* **2022**, *405*, 475−488.
(19) Valero, M. C.; Raybaud, P.; Sautet, P. Interplay between molecular adsorption and metal−support interaction for small supported metal clusters: CO and C2H4 adsorption on Pd4/γ-Al2O3. *J. Catal.* **2007**, *247* (2), 339−355.
(20) Kubička, D.; Kumar, N.; Venäläinen, T.; Karhu, H.; Kubičková, I.; Österholm, H.; Murzin, D. Y. Metal−Support Interactions in Zeolite-Supported Noble Metals: Influence of Metal Crystallites on the Support Acidity. *J. Phys. Chem. B* **2006**, *110* (10), 4937−4946.
(21) Kwak, J. H.; Hu, J.; Mei, D.; Yi, C.-W.; Kim, D. H.; Peden, C. H. F.; Allard, L. F.; Szanyi, J. Coordinatively Unsaturated Al3+ Centers as Binding Sites for Active Catalyst Phases of Platinum on gamma-Al2O3. *Science* **2009**, *325* (5948), 1670−1673.
(22) Vayssilov, G. N.; Gates, B. C.; Rösch, N. Oxidation of supported rhodium clusters by support hydroxy groups. *Angew. Chem., Int. Ed.* **2003**, *42* (12), 1391−1394.
(23) Hu, C. H.; Chizallet, C.; Mager-Maury, C.; Corral-Valero, M.; Sautet, P.; Toulhoat, H.; Raybaud, P. Modulation of catalyst particle structure upon support hydroxylation: Ab initio insights into Pd13 and Pt13/γ-Al2O3. *J. Catal.* **2010**, *274* (1), 99−110.
(24) Konda, S. S. M.; Caratzoulas, S.; Vlachos, D. G. Computational Insights into the Role of Metal and Acid Sites in Bifunctional Metal/Zeolite Catalysts: A Case Study of Acetone Hydrogenation to 2-Propanol and Subsequent Dehydration to Propene. *ACS Catal.* **2016**, *6* (1), 123−133.
(25) Vayssilov, G. N.; Lykhach, Y.; Migani, A.; Staudt, T.; Petrova, G. P.; Tsud, N.; Skála, T.; Bruix, A.; Illas, F.; Prince, K. C.; et al. Support nanostructure boosts oxygen transfer to catalytically active platinum nanoparticles. *Nat. Mater.* **2011**, *10* (4), 310−315.
(26) Weitkamp, J. Catalytic Hydrocracking−Mechanisms and Versatility of the Process. *ChemCatChem* **2012**, *4* (3), 292−306.
(27) Robinson, A. M.; Hensley, J. E.; Medlin, J. W. Bifunctional Catalysts for Upgrading of Biomass-Derived Oxygenates: A Review. *ACS Catal.* **2016**, *6* (8), 5026−5043.
(28) Liu, S.; Kots, P. A.; Vance, B. C.; Danielson, A.; Vlachos, D. G. Plastic waste to fuels by hydrocracking at mild conditions. *Sci. Adv.* **2021**, *7* (17), No. eabf8283.
(29) Zhang, L.; Zhou, M.; Wang, A.; Zhang, T. Selective hydrogenation over supported metal catalysts: from nanoparticles to single atoms. *Chem. Rev.* **2020**, *120* (2), 683−733.
(30) Aireddy, D. R.; Ding, K. Heterolytic Dissociation of H2 in Heterogeneous Catalysis. *ACS Catal.* **2022**, *12* (8), 4707−4723.
(31) Wan, W.; Nie, X.; Janik, M. J.; Song, C.; Guo, X. Adsorption, Dissociation, and Spillover of Hydrogen over Au/TiO2 Catalysts: The Effects of Cluster Size and Metal−Support Interaction from DFT. *J. Phys. Chem. C* **2018**, *122* (31), 17895−17916.
(32) Bariås, O. A.; Holmen, A.; Blekkan, E. A. Propane Dehydrogenation over Supported Pt and Pt−Sn Catalysts: Catalyst Preparation, Characterization, and Activity Measurements. *J. Catal.* **1996**, *158* (1), 1−12.
(33) Spreafico, C.; Karim, W.; Ekinci, Y.; van Bokhoven, J. A.; VandeVondele, J. Hydrogen Adsorption on Nanosized Platinum and Dynamics of Spillover onto Alumina and Titania. *J. Phys. Chem. C* **2017**, *121* (33), 17862−17872.
(34) Cavanagh, R. R.; Yates, J. T. Hydrogen spillover on alumina—A study by infrared spectroscopy. *J. Catal.* **1981**, *68* (1), 22−26.
(35) King, T. S.; Wu, X.; Gerstein, B. C. Direct evidence for spillover of hydrogen from ruthenium to copper in supported copper-ruthenium/silica catalysts: a study by NMR of chemisorbed hydrogen. *J. Am. Chem. Soc.* **1986**, *108* (19), 6056−6058.
(36) Wei, J.; Qin, S.-N.; Liu, J.-L.; Ruan, X.-Y.; Guan, Z.; Yan, H.; Wei, D.-Y.; Zhang, H.; Cheng, J.; Xu, H.; Tian, Z.-Q.; Li, J.-F. In Situ Raman Monitoring and Manipulating of Interfacial Hydrogen Spillover by Precise Fabrication of Au/TiO2/Pt Sandwich Structures. *Angew. Chem., Int. Ed.* **2020**, *59* (26), 10343−10347.
(37) Niemantsverdriet, J. W. *Spectroscopy in Catalysis: An Introduction*; John Wiley & Sons, 2007.
(38) Kresse, G.; Hafner, J. Ab initio molecular dynamics for liquid metals. *Phys. Rev. B* **1993**, *47* (1), 558−561.
(39) Kresse, G.; Furthmüller, J. Efficient iterative schemes for ab initio total-energy calculations using a plane-wave basis set. *Phys. Rev. B* **1996**, *54* (16), 11169−11186.
(40) Kresse, G.; Furthmüller, J. Efficiency of ab-initio total energy calculations for metals and semiconductors using a plane-wave basis set. *Comput. Mater. Sci.* **1996**, *6* (1), 15−50.
(41) Perdew, J. P.; Burke, K.; Ernzerhof, M. Generalized gradient approximation made simple. *Phys. Rev. Lett.* **1996**, *77* (18), 3865−3868.
(42) Grimme, S.; Antony, J.; Ehrlich, S.; Krieg, H. A consistent and accurate ab initio parametrization of density functional dispersion correction (DFT-D) for the 94 elements H-Pu. *J. Chem. Phys.* **2010**, *132* (15), 154104.

(43) Grimme, S.; Ehrlich, S.; Goerigk, L. Effect of the damping function in dispersion corrected density functional theory. *J. Comput. Chem.* **2011**, *32* (7), 1456−1465.
(44) Kresse, G.; Joubert, D. From ultrasoft pseudopotentials to the projector augmented-wave method. *Phys. Rev. B* **1999**, *59* (3), 1758−1775.
(45) Batchu, S. P.; Wang, H.-L.; Chen, W.; Zheng, W.; Caratzoulas, S.; Lobo, R. F.; Vlachos, D. G. Ethane Dehydrogenation on Single and Dual Centers of Ga-modified γ-Al2O3. *ACS Catal.* **2021**, *11* (3), 1380−1391.
(46) Monkhorst, H. J.; Pack, J. D. Special points for Brillouin-zone integrations. *Phys. Rev. B* **1976**, *13* (12), 5188−5192.
(47) Dronskowski, R.; Bloechl, P. E. Crystal orbital Hamilton populations (COHP): energy-resolved visualization of chemical bonding in solids based on density-functional calculations. *J. Phys. Chem.* **1993**, *97* (33), 8617−8624.
(48) Deringer, V. L.; Tchougréeff, A. L.; Dronskowski, R. Crystal Orbital Hamilton Population (COHP) Analysis As Projected from Plane-Wave Basis Sets. *J. Phys. Chem. A* **2011**, *115* (21), 5461−5466.
(49) Maintz, S.; Deringer, V. L.; Tchougréeff, A. L.; Dronskowski, R. Analytic projection from plane-wave and PAW wavefunctions and application to chemical-bonding analysis in solids. *J. Comput. Chem.* **2013**, *34* (29), 2557−2567.
(50) Maintz, S.; Deringer, V. L.; Tchougréeff, A. L.; Dronskowski, R. LOBSTER: A tool to extract chemical bonding from plane-wave based DFT. *J. Comput. Chem.* **2016**, *37* (11), 1030−1035.
(51) Maintz, S.; Esser, M.; Dronskowski, R. Efficient Rotation of Local Basis Functions Using Real Spherical Harmonics. *Acta Phys. Pol. B* **2016**, *47* (4), 1165−1175.
(52) Nelson, R.; Ertural, C.; George, J.; Deringer, V. L.; Hautier, G.; Dronskowski, R. LOBSTER: Local orbital projections, atomic charges, and chemical-bonding analysis from projector-augmented-wave-based density-functional theory. *J. Comput. Chem.* **2020**, *41* (21), 1931−1940.
(53) Behler, J.; Csányi, G. Machine learning potentials for extended systems: a perspective. *Eur. Phys. J. B* **2021**, *94* (7), 142.
(54) Deringer, V. L.; Caro, M. A.; Csányi, G. Machine Learning Interatomic Potentials as Emerging Tools for Materials Science. *Adv. Mater.* **2019**, *31* (46), 1902765.
(55) Shapeev, A. V. Moment Tensor Potentials: A Class of Systematically Improvable Interatomic Potentials. *Multiscale Model. Simul.* **2016**, *14* (3), 1153−1173.
(56) Zuo, Y.; Chen, C.; Li, X.; Deng, Z.; Chen, Y.; Behler, J.; Csányi, G.; Shapeev, A. V.; Thompson, A. P.; Wood, M. A.; Ong, S. P. Performance and Cost Assessment of Machine Learning Interatomic Potentials. *J. Phys. Chem. A* **2020**, *124* (4), 731−745.
(57) Novikov, I. S.; Gubaev, K.; Podryabinkin, E. V.; Shapeev, A. V. The MLIP package: moment tensor potentials with MPI and active learning. *Mach. Learn.: Sci. Technol.* **2021**, *2* (2), 025002.
(58) Thompson, A. P.; Aktulga, H. M.; Berger, R.; Bolintineanu, D. S.; Brown, W. M.; Crozier, P. S.; in 't Veld, P. J.; Kohlmeyer, A.; Moore, S. G.; Nguyen, T. D.; Shan, R.; Stevens, M. J.; Tranchida, J.; Trott, C.; Plimpton, S. J. LAMMPS - a flexible simulation tool for particle-based materials modeling at the atomic, meso, and continuum scales. *Comput. Phys. Commun.* **2022**, *271*, 108171.
(59) Frenkel, D.; Smit, B. *Understanding Molecular Simulation: From Algorithms to Applications*; Elsevier Science, 2023.
(60) Schneider, T.; Stoll, E. Molecular-dynamics study of a three-dimensional one-component model for distortive phase transitions. *Phys. Rev. B* **1978**, *17* (3), 1302−1322.
(61) Vaarkamp, M.; Miller, J. T.; Modica, F. S.; Koningsberger, D. C. On the Relation between Particle Morphology, Structure of the Metal-Support Interface, and Catalytic Properties of Pt/γ-Al2O3. *J. Catal.* **1996**, *163* (2), 294−305.
(62) Khan, S. A.; Caratzoulas, S.; Vlachos, D. G. Catalyst Cluster-Induced Support Restructuring. *J. Phys. Chem. C* **2023**, *127* (45), 22277−22286.
(63) Meyers, R. A. *Handbook of Petroleum Refining Processes*; McGraw Hill Professional, 2004; .
(64) Goldsmith, B. R.; Florian, J.; Liu, J.-X.; Gruene, P.; Lyon, J. T.; Rayner, D. M.; Fielicke, A.; Scheffler, M.; Ghiringhelli, L. M. Two-to-three dimensional transition in neutral gold clusters: The crucial role of van der Waals interactions and temperature. *Phys. Rev. Mater.* **2019**, *3* (1), 016002.
(65) Gong, F.-Q.; Guo, Y.-X.; Fan, Q.-Y.; Cheng, J. Dynamic catalysis of sub-nanometer metal clusters in oxygen dissociation. *Next Nanotechnology* **2023**, *1*, 100002.
(66) Farigliano, L. M.; Villarreal, M. A.; Leiva, E. P. M.; Paz, S. A. Thermodynamics of Nanoparticle Coalescence at Different Temperatures via Well-Tempered Metadynamics. *J. Phys. Chem. C* **2020**, *124* (43), 24009−24016.
(67) Sun, G.; Alexandrova, A. N.; Sautet, P. Pt8 cluster on alumina under a pressure of hydrogen: Support-dependent reconstruction from first-principles global optimization. *J. Chem. Phys.* **2019**, *151* (19), 194703.
(68) Wang, Y.-G.; Mei, D.; Glezakou, V.-A.; Li, J.; Rousseau, R. Dynamic formation of single-atom catalytic active sites on ceria-supported gold nanoparticles. *Nat. Commun.* **2015**, *6* (1), 6511.
(69) Hoffmann, R. A chemical and theoretical way to look at bonding on surfaces. *Rev. Mod. Phys.* **1988**, *60* (3), 601−628.
(70) Chiesa, M.; Paganini, M. C.; Giamello, E.; Di Valentin, C.; Pacchioni, G. First Evidence of a Single-Ion Electron Trap at the Surface of an Ionic Oxide. *Angew. Chem., Int. Ed.* **2003**, *42* (15), 1759−1761.
(71) Chiesa, M.; Paganini, M. C.; Giamello, E.; Murphy, D. M.; Di Valentin, C.; Pacchioni, G. Excess Electrons Stabilized on Ionic Oxide Surfaces. *Acc. Chem. Res.* **2006**, *39* (11), 861−867.
(72) Wischert, R.; Laurent, P.; Copéret, C.; Delbecq, F.; Sautet, P. γ-Alumina: The Essential and Unexpected Role of Water for the Structure, Stability, and Reactivity of "Defect" Sites. *J. Am. Chem. Soc.* **2012**, *134* (35), 14430−14449.
(73) Haq, S.; King, D. A. Configurational Transitions of Benzene and Pyridine Adsorbed on Pt{111} and Cu{110} Surfaces: An Infrared Study. *J. Phys. Chem.* **1996**, *100* (42), 16957−16965.
(74) Kolsbjerg, E. L.; Groves, M. N.; Hammer, B. Pyridine adsorption and diffusion on Pt(111) investigated with density functional theory. *J. Chem. Phys.* **2016**, *144* (16), 164112.
(75) Ahmed, F.; Alam, M. K.; Suzuki, A.; Koyama, M.; Tsuboi, H.; Hatakeyama, N.; Endou, A.; Takaba, H.; Del Carpio, C. A.; Kubo, M.; Miyamoto, A. Dynamics of Hydrogen Spillover on Pt/γ-Al2O3 Catalyst Surface: A Quantum Chemical Molecular Dynamics Study. *J. Phys. Chem. C* **2009**, *113* (35), 15676−15683.
(76) Gu, K.; Li, C.; Jiang, B.; Lin, S.; Guo, H. Short- and Long-Time Dynamics of Hydrogen Spillover from a Single Atom Platinum Active Site to the Cu(111) Host Surface. *J. Phys. Chem. C* **2022**, *126* (40), 17093−17101.
(77) Ahmed, F.; Alam, M. K.; Muira, R.; Suzuki, A.; Tsuboi, H.; Hatakeyama, N.; Endou, A.; Takaba, H.; Kubo, M.; Miyamoto, A. Adsorption and dissociation of molecular hydrogen on Pt/CeO2 catalyst in the hydrogen spillover process: A quantum chemical molecular dynamics study. *Appl. Surf. Sci.* **2010**, *256* (24), 7643−7652.
(78) Prins, R. Hydrogen Spillover. Facts and Fiction. *Chem. Rev.* **2012**, *112* (5), 2714−2738.
(79) Im, J.; Shin, H.; Jang, H.; Kim, H.; Choi, M. Maximizing the catalytic function of hydrogen spillover in platinum-encapsulated aluminosilicates with controlled nanostructures. *Nat. Commun.* **2014**, *5* (1), 3370.
(80) Beaumont, S. K.; Alayoglu, S.; Specht, C.; Kruse, N.; Somorjai, G. A. A Nanoscale Demonstration of Hydrogen Atom Spillover and Surface Diffusion Across Silica Using the Kinetics of CO2 Methanation Catalyzed on Spatially Separate Pt and Co Nanoparticles. *Nano Lett.* **2014**, *14* (8), 4792−4796.
(81) Karim, W.; Spreafico, C.; Kleibert, A.; Gobrecht, J.; VandeVondele, J.; Ekinci, Y.; van Bokhoven, J. A. Catalyst support effects on hydrogen spillover. *Nature* **2017**, *541* (7635), 68−71.
(82) Mager-Maury, C.; Bonnard, G.; Chizallet, C.; Sautet, P.; Raybaud, P. H2-Induced Reconstruction of Supported Pt Clusters:

Metal−Support Interaction versus Surface Hydride. *ChemCatChem* **2011**, *3* (1), 200−207.
(83) Gorczyca, A.; Moizan, V.; Chizallet, C.; Proux, O.; Del Net, W.; Lahera, E.; Hazemann, J.-L.; Raybaud, P.; Joly, Y. Monitoring Morphology and Hydrogen Coverage of Nanometric Pt/γ-Al2O3 Particles by In Situ HERFD−XANES and Quantum Simulations. *Angew. Chem., Int. Ed.* **2014**, *53* (46), 12426−12429.
(84) Vottero, E.; Carosso, M.; Ricchebuono, A.; Jiménez-Ruiz, M.; Pellegrini, R.; Chizallet, C.; Raybaud, P.; Groppo, E.; Piovano, A. Evidence for H2-Induced Ductility in a Pt/Al2O3 Catalyst. *ACS Catal.* **2022**, *12* (10), 5979−5989.
(85) Alexeev, O.; Kim, D.-W.; Graham, G. W.; Shelef, M.; Gates, B. C. Temperature-Programmed Desorption of Hydrogen from Platinum Particles on γ-Al2O3: Evidence of Platinum-Catalyzed Dehydroxylation of γ-Al2O3. *J. Catal.* **1999**, *185* (1), 170−181.
(86) Fu, Q.; Wagner, T. Interaction of nanostructured metal overlayers with oxide surfaces. *Surf. Sci. Rep.* **2007**, *62* (11), 431−498.
(87) Xu, D.; Zhang, S.-N.; Chen, J.-S.; Li, X.-H. Design of the Synergistic Rectifying Interfaces in Mott−Schottky Catalysts. *Chem. Rev.* **2023**, *123* (1), 1−30.
(88) Prada, S.; Martinez, U.; Pacchioni, G. Work function changes induced by deposition of ultrathin dielectric films on metals: A theoretical analysis. *Phys. Rev. B* **2008**, *78* (23), 235423.
(89) Goniakowski, J.; Noguera, C. Electronic States and Schottky Barrier Height at Metal/MgO(100) Interfaces. *Interface Sci.* **2004**, *12* (1), 93−103.
(90) Pacchioni, G.; Freund, H.-J. Controlling the charge state of supported nanoparticles in catalysis: lessons from model systems. *Chem. Soc. Rev.* **2018**, *47* (22), 8474−8502.
(91) Schintke, S.; Messerli, S.; Pivetta, M.; Patthey, F.; Libioulle, L.; Stengel, M.; De Vita, A.; Schneider, W.-D. Insulator at the Ultrathin Limit: MgO on Ag(001). *Phys. Rev. Lett.* **2001**, *87* (27), 276801.
(92) Giordano, L.; Baistrocchi, M.; Pacchioni, G. Bonding of Pd, Ag, and Au atoms on MgO(100) surfaces and MgO/Mo(100) ultra-thin films: A comparative DFT study. *Phys. Rev. B* **2005**, *72* (11), 115403.
(93) Chen, H.-Y. T.; Tosoni, S.; Pacchioni, G. Hydrogen Adsorption, Dissociation, and Spillover on Ru10 Clusters Supported on Anatase TiO2 and Tetragonal ZrO2 (101) Surfaces. *ACS Catal.* **2015**, *5* (9), 5486−5495.
(94) Mehta, P.; Greeley, J.; Delgass, W. N.; Schneider, W. F. Adsorption Energy Correlations at the Metal−Support Boundary. *ACS Catal.* **2017**, *7* (7), 4707−4715.
(95) Choksi, T.; Majumdar, P.; Greeley, J. P. Electrostatic Origins of Linear Scaling Relationships at Bifunctional Metal/Oxide Interfaces: A Case Study of Au Nanoparticles on Doped MgO Substrates. *Angew. Chem., Int. Ed.* **2018**, *57* (47), 15410−15414.
(96) Del Vitto, A.; Pacchioni, G.; Delbecq, F.; Sautet, P. Au Atoms and Dimers on the MgO(100) Surface: A DFT Study of Nucleation at Defects. *J. Phys. Chem. B* **2005**, *109* (16), 8040−8048.
(97) Pan, Y.; Nilius, N.; Freund, H.-J.; Paier, J.; Penschke, C.; Sauer, J. Titration of Ce 3+ ions in the CeO 2 (111) surface by Au adatoms. *Phys. Rev. Lett.* **2013**, *111* (20), 206101.
(98) Korpelin, V.; Melander, M. M.; Honkala, K. Reducing the Irreducible: Dispersed Metal Atoms Facilitate Reduction of Irreducible Oxides. *J. Phys. Chem. C* **2022**, *126* (2), 933−945.
(99) Frondelius, P.; Hellman, A.; Honkala, K.; Häkkinen, H.; Grönbeck, H. Charging of atoms, clusters, and molecules on metal-supported oxides: A general and long-ranged phenomenon. *Phys. Rev. B* **2008**, *78* (8), 085426.
(100) Gonchar, A.; Risse, T.; Freund, H.-J.; Giordano, L.; Di Valentin, C.; Pacchioni, G. Activation of Oxygen on MgO: O2.− Radical Ion Formation on Thin, Metal-Supported MgO(001) Films. *Angew. Chem., Int. Ed.* **2011**, *50* (11), 2635−2638.
(101) Chen, H.-Y. T.; Giordano, L.; Pacchioni, G. From Heterolytic to Homolytic H2 Dissociation on Nanostructured MgO(001) Films As a Function of the Metal Support. *J. Phys. Chem. C* **2013**, *117* (20), 10623−10629.
(102) Giordano, L.; Pacchioni, G. Charge transfers at metal/oxide interfaces: a DFT study of formation of Kδ+ and Auδ− species on MgO/Ag(100) ultra-thin films from deposition of neutral atoms. *Phys. Chem. Chem. Phys.* **2006**, *8* (28), 3335−3341.
(103) Andersen, M.; Medford, A. J.; Nørskov, J. K.; Reuter, K. Analyzing the Case for Bifunctional Catalysis. *Angew. Chem., Int. Ed.* **2016**, *55* (17), 5210−5214.
(104) Andersen, M.; Medford, A. J.; Nørskov, J. K.; Reuter, K. Scaling-Relation-Based Analysis of Bifunctional Catalysis: The Case for Homogeneous Bimetallic Alloys. *ACS Catal.* **2017**, *7* (6), 3960−3967.
(105) Wang, S.; Vorotnikov, V.; Vlachos, D. G. Coverage-induced conformational effects on activity and selectivity: hydrogenation and decarbonylation of furfural on Pd(111). *ACS Catal.* **2015**, *5* (1), 104−112.
(106) Saerens, S.; Sabbe, M. K.; Galvita, V. V.; Redekop, E. A.; Reyniers, M.-F.; Marin, G. B. The Positive Role of Hydrogen on the Dehydrogenation of Propane on Pt(111). *ACS Catal.* **2017**, *7* (11), 7495−7508.
(107) Molina, L. M.; Hammer, B. Active Role of Oxide Support during CO Oxidation at Au/MgO. *Phys. Rev. Lett.* **2003**, *90* (20), 206102.
(108) Foppa, L.; Margossian, T.; Kim, S. M.; Müller, C.; Copéret, C.; Larmier, K.; Comas-Vives, A. Contrasting the Role of Ni/Al2O3 Interfaces in Water−Gas Shift and Dry Reforming of Methane. *J. Am. Chem. Soc.* **2017**, *139* (47), 17128−17139.
(109) Silaghi, M.-C.; Comas-Vives, A.; Copéret, C. CO2 Activation on Ni/γ−Al2O3 Catalysts by First-Principles Calculations: From Ideal Surfaces to Supported Nanoparticles. *ACS Catal.* **2016**, *6* (7), 4501−4505.

https://doi.org/10.1021/acscatal.4c03485
ACS Catal. 2024, 14, 13579−13590